Magnetic spin structure of pyroxene-type $MnGeO_3$

2011 J. Phys.: Condens. Matter 23 254202

(http://iopscience.iop.org/0953-8984/23/25/254202)

IOP Publishing Journal of Physics: Condensed Matter

J. Phys.: Condens. Matter **23** (2011) 254202 (11pp) doi:10.1088/0953-8984/23/25/254202

Magnetic spin structure of pyroxene-type $MnGeO_3$

G J Redhammer[1], A Senyshyn[2], G Tippelt[1] and G Roth[3]

[1] Division of Mineralogy, Department of Materials Engineering and Physics, University of Salzburg, Hellbrunnertstr. 34, A-5020 Salzburg, Austria
[2] Institute for Materials Science, Darmstadt University of Technology, Petersenstrasse 23, 64287 Darmstadt, c/o Forschungs-Neutronenquelle Heinz Maier-Leibnitz FRM II, Lichtenbergstrasse 1, 85747 Garching, Germany
[3] Institute of Crystallography, RWTH Aachen University, Jägerstraße 17/19, D-52056 Aachen, Germany

E-mail: guenther.redhammer@sbg.ac.at

Received 14 January 2011, in final form 14 February 2011
Published 8 June 2011
Online at stacks.iop.org/JPhysCM/23/254202

Abstract

Polycrystalline $MnGeO_3$ material was synthesized at 1473 K and ambient pressures using ceramic sintering techniques. Under these conditions the pyroxene-type compound crystallizes in the orthorhombic modification with space group $Pbca$, as determined from the refinement of the neutron diffraction data. The monoclinic modification, space group $C2/c$, was also present at a level of 8.8(4) wt% and the magnetic structures for the two polymorphs at low temperatures have been found simultaneously. The monoclinic form orders magnetically below 34 K; the spin structure can be described using $\boldsymbol{k} = (0, 0, 0)$ in the magnetic space group $C2'/c$, having an antiferromagnetic spin arrangement within and between the chains of M1 and M2 sites. The orthorhombic phase of $MnGeO_3$ transforms to a magnetically ordered state with $\boldsymbol{k} = (0, 0, 0)$ and magnetic space group $Pb'c'a$ below 12 K. Spins on M1 sites are aligned along the crystallographic $\boldsymbol{a}$-axis with a slight non-collinear antiferromagnetic spin arrangement with and between the M1 chains. Spins on M2 sites are also antiferromagnetically coupled; however, one of the three different M1–M2 superexchange pathways within the band of M1 and M2 sites displays a ferromagnetic interaction, while the other two allow antiferromagnetic interaction.

S Online supplementary data available from stacks.iop.org/JPhysCM/23/254202/mmedia

(Some figures in this article are in colour only in the electronic version)

1. Introduction

Pyroxenes, well known as rock forming minerals in the upper mantle of planet Earth and frequently studied in geosciences owing to their rich crystal chemistry (e.g. [1–3]), also display a wide variety of different magnetic ground states. The specific structural topology of the pyroxenes with infinite quasi-1D chains of transition-metal bearing M1 sites and M1–O–M1 angles close to 90° and their interconnection via infinite chains of corner-sharing TO_4 tetrahedra causes a competitive interaction between magnetic coupling within and between these M1 chains, which—finally—determines the bulk magnetic properties. The quite open architecture of the pyroxene structure allows tailoring geometry and distances within and between the M1 chains by chemical substitutions on M2 and tetrahedral sites while keeping the type of a magnetic active transition metal on the M1 site unchanged. Thereby it is possible to introduce small alterations to the crystal structure, which, however, can cause drastic alterations in magnetic properties. This feature and the discovery of multiferroic behaviour by Jodlauk *et al* [4], have increased interest in pyroxenes also in the fields of solid state physics. The variety of magnetic ground states is large, with compounds with pure antiferromagnetic interactions in and between the M1 chains as in $CaMnGe_2O_6$ [5], pure ferromagnetic interactions as in $NaCrGe_2O_6$ [6], mixtures between the two [5, 7–9], and even compounds with spin-gap behaviour as in $NaTiSi_2O_6$ [10, 11]. Of particular interest are four-components systems such as the $(Na, Li)Fe(Si, Ge)_2O_6$ series: the compound $LiFeSi_2O_6$ has a simple magnetic

structure with a ferromagnetic (FM) coupling of spins within the M1 chains and an antiferromagnetic (AFM) one between the chains [8]. In the analogue germanate the interaction within the chains changes to AFM, while between the chains there is an alteration from AFM and FM coupling, depending on the interaction via the two structurally distinct GeA and GeB sites; thus the magnetic unit cell becomes doubled along the ***a***-axis. $NaFeGe_2O_6$ possesses a complicated incommensurately modulated cyclical/ helical magnetic structure below 19 K [12] and multiferroic $NaFeSi_2O_6$ first transforms to a commensurate magnetic structure with an FM coupling within and an AFM coupling between the M1 chains around 8 K, but changes to an incommensurately modulated structure below 6 K [4, 12]. Also in the $(Na, Li)Cr(Si, Ge)_2O_6$ series, small structural alterations change the magnetic properties, however, only simple magnetic structures are realized here [6, 13, 14]. As a continuation of our ongoing research on magnetism in pyroxenes [5, 7–9, 12, 15, 16] this study is devoted to (i) the investigation of the spin structure of $MnGeO_3$ with the orthopyroxene structure using high resolution neutron powder data and (ii) a comparison to the compound $CaMnGe_2O_6$ [5] having the M2 site filled with the larger diamagnetic Ca^{2+} and thus the M1 chains more separated from each other.

$MnGeO_3$ itself was first reported by Tauber *et al* [17] as an analogue to the mineral enstatite $MgSiO_3$. The crystal structure was described later on by Fang *et al* [18] to have orthorhombic symmetry, space group $Pbca$; some new x-ray data on flux grown single crystals are included in Sapronova *et al* [19]. Matsumura *et al* [20] were not able to synthesize pure $MnGeO_3$ as large boules with the floating-zone method; the large crystals disintegrated into small pieces upon cooling; the authors argue that this behaviour is due to the orthorhombic to monoclinic phase transition taking place at around 473 K. In the fragments of the large crystals they found untwined parts of the orthorhombic and finely twined parts of the monoclinic $MnGeO_3$-structure. So both, the monoclinic $C2/c$ as well as the orthorhombic $Pbca$ form of $MnGeO_3$, exist at room temperature, at least in a metastable state, this is similar to the isotypic $CoGeO_3$, recently described in full detail in [9].

Disagreement exists concerning the magnetic ordering temperature T_N of $MnGeO_3$. On a powder sample of orthorhombic $MnGeO_3$ Herpin *et al* [21] found magnetic ordering below 16 K in their neutron diffraction experiments with the magnetic moment aligned along the ***b***-axis; the magnetic space group was given as $Pb'ca$. Brown *et al* [22] detected antiferromagnetic ordering below 8 K in a single crystal with $Mn_{0.94}Mg_{0.06}GeO_3$ having the spins aligned along ***b***, but they found an additional transition to an incommensurate phase below 4.5 K. These low ordering temperatures contrast the Neél temperatures determined on flux grown single crystals of orthorhombic $MnGeO_3$ of [19] with magnetic ordering temperatures around 38 K. Powdered single crystals gave identical ordering temperatures. Sapranova *et al* [19] argued that these distinct differences may be due to the preparation method and the fact that $MnGeO_3$ with low T_N was prepared in silica tubes and probably has Ge^{4+} replaced by Si^{4+}, thereby lowering T_N. This is supported by an experiment described in [19] were the authors synthesized a pyroxene with $MnGe_{1.88}Si_{0.12}O_3$ having $T_N \sim 18$ K. So, along with the redetermination of the magnetic spin structure of $MnGeO_3$ an additional goal of this study is to shed some light onto the origin of the different magnetic ordering temperatures that had been observed.

2. Experimental details

2.1. Materials synthesis

$MnGeO_3$ was prepared in a 15 g batch from the appropriate proportions of MnO and GeO_2 using a ceramic sintering route. A surplus of 2.5 wt% GeO_2 was added to account for possible loss of Ge at temperatures above 1373 K [23]. Before synthesis the starting material was carefully homogenized by grinding in an agate mortar under alcohol, pressed to pellets (∼2 g each), put into an open platinum crucible and transferred to a high temperature chamber furnace (LINN VMK). $MnGeO_3$ was fired at 1473 K under atmospheric pressure over a period of 18 days with three intermediate regrinding/repressing steps. The final sample had a beige brown colour and contained $MnGeO_3$ only. During neutron diffraction work, however, it turned out that the sample mainly consists of the orthorhombic phase with 8.5(4) wt% of the monoclinic modification.

2.2. Neutron diffraction

Neutron diffraction experiments were done at the Heinz Maier-Leibnitz Forschungs-Neutronenquelle (FRM II) Munich, Germany. Powder diffraction data were acquired in constant wavelength mode using the high resolution powder diffractometer SPODI [24] on the sample contained in a 14 mm diameter vanadium can at temperatures between 4 and 50 K with Ge331 monochromatized neutron radiation ($\lambda = 2.537$ Å) and between 50 and 300 K with Ge551 monochromatized neutron radiation ($\lambda = 1.549$ Å). Experiments were performed in a 2θ range $3° \leqslant 2\theta \leqslant 152°$, step width 0.04°. Data treatment (k-vector determination, Rietveld refinement) was done using the FullProf suite of programs [25] and the structural data of $CoGeO_3$ [9] were taken as starting parameters in Rietveld refinements. Experimental data and refinement results of the 4, 50 and 298 K measurements for both modifications are compiled in table 1, fractional atomic coordinates are listed in table 2 and some secondary structural parameters are listed in table 3.

2.3. High temperature x-ray diffraction

To obtain information on the high temperature variation of the lattice parameters and possible symmetry changes, powder x-ray diffraction measurements (5°–100° in 2θ, continuous scan mode) were carried out in the temperature range 295–1273 K. Data were collected on a Philips X'Pert diffractometer system, equipped with an Anton PAAR HTK-16 high temperature chamber (Cu Kα radiation, primary and secondary side 0.04 rad Soller slits, secondary graphite monochromator, 4 h/measurement). After each temperature increase the sample was allowed to equilibrate for 1 h before starting measurement at this temperature. In order to parameterize the cell parameter

Table 1. Experimental details and results of Rietveld refinements of the constant wavelength neutron diffraction pattern of $MnGeO_3$ in the monoclinic and the orthorhombic form at some selected temperatures. (For all data: constant wavelength step scan neutron data, SPODI diffractometer (FRM II, Germany) with $2\theta_{min} = 0.9°$, $2\theta_{max} = 151.9°$, step size = 0.04°; refinement of F^2, pseudo-Voigt function, no excluded regions.)

Sample	$MnGeO_3$			$MnGeO_3$		
Setting	Monoclinic			Orthorhombic		
T (K)	4	50	298	4	50	298
λ (Å)	2.537	1.549	1.549	2.537	1.549	1.549
S.G.	*C*2/*c*	*C*2/*c*	*C*2/*c*	*Pbca*	*Pbca*	*Pbca*
a (Å)	9.9007(10)	9.8995(10)	9.9138(10)	19.2776(2)	19.2717(2)	19.2864(2)
b (Å)	9.2572(10)	9.2586(9)	9.2733(10)	9.2409(1)	9.2394(1)	9.2548(1)
c (Å)	5.2655(5)	5.2682(6)	5.2738(6)	5.4676(1)	5.4715(1)	5.4782(1)
β (Å)	101.47(1)	101.50(1)	101.66(1)	—	—	—
V (Å^3)	472.95(8)	473.16(9)	474.84(8)	973.99(2)	974.25(2)	977.81(2)
R_p (%)	3.08	2.28	2.14	3.08	2.28	2.14
R_{wp} (%)	3.67	2.79	2.60	3.67	2.79	2.60
R_{exp} (%)	1.61	1.52	1.56	1.61	1.52	1.56
R_B (%)	1.40	2.22	2.70	1.44	1.70	1.85
R_{magn} (%)	3.16	—	—	2.53	—	—
wt%	8.8(4)	8.7(3)	8.8(3)	91.2(7)	91.3(3)	91.2(3)

variation for thermal expansion tensor calculations, the data were fitted to a simple quasi-harmonic Einstein model [3, 9] and according to

$$a = a_0 + \frac{C_E}{e^{(\theta_E/T)} - 1} \quad (1)$$

(where a_0 is the unit cell dimension at 0 K, C_E is a constant and θ_E is the temperature above which saturation is reached and the thermal expansion can be considered as constant. Results of the fitting procedure are compiled in table 4). The method employed for calculating thermal expansion coefficients from lattice parameters is described in detail elsewhere [3, 9]. During high temperature data collection it was found that between 1123 and 1173 K the impurity of the monoclinic phase disappeared, lowering temperature below these temperatures, however, did not bring the monoclinic phase back[4]. Therefore we conclude that around 1123 K there is a non-reversible phase transition of the monoclinic to the orthorhombic phase in $MnGeO_3$. Further synthesis and *in situ* experiments are needed to clarify these effects. Generally we do not find any structural phase transition around 473 K (at least, not within the time frame of our experiments), that had been described in the literature [19, 20].

3. Results

3.1. Crystal structure at 298 K

The orthorhombic modification of $MnGeO_3$ crystallizes in space group *Pbca*. It is isotypic to $CoGeO_3$ [9] and $MgGeO_3$ [26]. Lattice parameters are distinctly larger in the title compound reflecting the substitution of smaller Mg or Co^{2+} by the large Mn^{2+} cation. The general topology of orthorhombic $MnGeO_3$ structure is similar to the one in $CoGeO_3$ [9] and can be described as follows (figures 1(a) and (b)). The two distinct Ge sites, GeA and GeB are tetrahedrally coordinated by oxygen atoms and form infinite chains, running parallel to the ***c***-axis. These are characterized by different tetrahedral kinking angles: the GeA chain is more stretched with a larger bridging angle O3A–O3A–O3A of 160.30° while the GeB chain is more kinked with O3B–O3B–O3B = 134.86°. These angles are larger than in $CoGeO_3$, as are the average ⟨Ge–O⟩ bond lengths and polyhedral volumes. The incorporation of the large Mn^{2+} cation thus is balanced by both, stretching of the tetrahedral chains and Ge–O bond length alteration. As generally observed [1, 9, 26], the GeB site is somewhat larger than the GeA site (table 3).

The tetrahedral chains interconnect the transition-metal bearing M1/M2 bands to each other. The M1 sites consist of regular oxygen atom octahedra with ⟨Mn1–O⟩ = 2.181(4) Å, forming infinite zigzag chains parallel to the crystallographic ***c***-axis by sharing two edges with two neighbouring M1-polyhedra. The M2 site is six-fold coordinated by oxygen atoms forming an irregularly shaped octahedron with ⟨Mn2–O⟩ = 2.240(4) Å. Four shorter bonds lie between 2.079(4) and 2.192(4) Å, while the oxygen atoms O3A and O3B which are part of the tetrahedral chains, form longer bonds with 2.38 . . . and 2.458 A. On alternating sides of the M1 chains, the M2 sites are attached to the M1 chain via three common edges, thus forming bands of M1 and M2 sites; there is no direct connection between individual M2 sites (figure 1).

Pyroxenes are often referred to as quasi-1D systems. This is because of the distinct chain-like character of transition-metal bearing building units (M1 sites) and their large separation (here by GeO_4 tetrahedral chains) from each other. With respect to magnetic ordering dominated by the magnetic superexchange between transition metal cations, the M–M distances and the M–O–M bond angles are of importance (table 3). Within the M1 chain, the shortest Mn^{2+}–Mn^{2+} distance is 3.269(3) Å, this exchange path is usually denoted as J. Two bond angles are involved in this interaction: Mn1–O1B–Mn1 = 94.67(4)° and Mn1–O1A–Mn1 = 96.17(4)°;

[4] A figure with the corresponding measurements is available as supplementary material (available at stacks.iop.org/JPhysCM/23/254202/mmedia) from the journals homepage.

Table 2. Fractional atomic coordinates and equivalent atomic displacement parameters for $MnGeO_3$ at three selected temperatures, as extracted from Rietveld refinements of neutron diffraction data.

Name	*x*	*y*	*z*	*B*
Pbca phase, $T = 300$ K				
Mn1	0.1235(2)	0.3463(4)	0.3609(4)	0.53(4)
Mn2	0.3776(2)	0.4833(3)	0.3531(5)	0.32(4)
Ge1	0.270 76(6)	0.3431(2)	0.0338(2)	0.43(2)
Ge2	0.472 82(6)	0.1617(2)	0.2988(2)	0.42(2)
O1A	0.180 79(8)	0.3405(3)	0.0235(3)	0.65(32)
O2A	0.309 71(10)	0.5098(2)	0.0441(3)	0.77(3)
O3A	0.305 48(9)	0.2243(2)	0.8147(3)	0.72(3)
O1B	0.563 15(10)	0.3401(3)	0.8037(3)	0.63(3)
O2B	0.432 42(10)	0.4851(2)	0.6797(4)	0.72(3)
O3B	0.445 41(9)	0.1885(2)	0.6083(3)	0.61(3)
Pbca phase, $T = 50$ K				
Mn1	0.1233(1)	0.3457(3)	0.3601(4)	0.24(4)
Mn2	0.3776(1)	0.4828(3)	0.3497(5)	0.05(4)
Ge1	0.270 58(6)	0.3432(2)	0.0330(2)	0.17(2)
Ge2	0.472 52(5)	0.1622(2)	0.2993(2)	0.14(2)
O1A	0.180 73(7)	0.3402(3)	0.0221(3)	0.27(3)
O2A	0.309 44(9)	0.5102(2)	0.0423(3)	0.34(3)
O3A	0.305 77(9)	0.2234(2)	0.8148(3)	0.34(3)
O1B	0.563 08(9)	0.3398(3)	0.8046(3)	0.33(3)
O2B	0.432 42(9)	0.4855(2)	0.6787(4)	0.33(3)
O3B	0.445 32(8)	0.1878(2)	0.6095(3)	0.27(3)
Pbca phase, $T = 4$ K				
Mn1	0.1228(2)	0.3456(5)	0.3592(6)	0.46(9)
Mn2	0.3777(2)	0.4818(5)	0.3487(7)	0.18(10)
Ge1	0.2701(1)	0.3425(3)	0.0324(3)	0.33(5)
Ge2	0.472 75(9)	0.1634(3)	0.2987(3)	0.33(4)
O1A	0.1808(1)	0.3393(5)	0.0232(5)	0.63(7)
O2A	0.3089(2)	0.5105(3)	0.0401(5)	0.99(7)
O3A	0.3056(1)	0.2244(3)	0.8147(4)	0.65(7)
O1B	0.5624(1)	0.3401(4)	0.8059(4)	0.44(6)
O2B	0.4316(2)	0.4860(3)	0.6784(6)	0.42(6)
O3B	0.4453(1)	0.1879(4)	0.6118(4)	0.54(7)
*C*2/*c* phase, $T = 300$ K				
Mn1	0	0.8989(26)	0.25	0.15(6)
Mn2	0	0.2752(26)	0.25	1.06(19)
Ge1	0.2983(6)	0.0908(10)	0.2162(11)	1.45(6)
O1	0.1228(7)	0.0992(14)	0.1385(18)	1.19(9)
O2	0.3803(9)	0.2366(16)	0.3717(26)	2.27(13)
O3	0.3571(9)	0.0675(13)	0.9148(18)	2.05(12)
*C*2/*c* phase, $T = 50$ K				
Mn1	0	0.9028(28)	0.25	0.60(14)
Mn2	0	0.2702(21)	0.25	0.22(15)
Ge1	0.2996(6)	0.0920(9)	0.2133(11)	0.89(90)
O1	0.1216(9)	0.0982(13)	0.1383(17)	1.03(15)
O2	0.3772(9)	0.2353(12)	0.3751(22)	1.12(19)
O3	0.3549(8)	0.0640(12)	0.9175(18)	1.82(11)
*C*2/*c* phase, $T = 4$ K				
Mn1	0	0.8898(39)	0.25	0.50
Mn2	0	0.2749(33)	0.25	0.80
Ge1	0.2998(11)	0.0947(13)	0.2117(30)	0.35(13)
O1	0.1169(14)	0.0967(32)	0.1421(31)	0.83(19)
O2	0.3786(21)	0.2402(25)	0.3716(40)	1.73(28)
O3	0.3566(18)	0.0671(20)	0.9155(40)	1.80(24)

both are well above the 90° M–O–M, favouring ferromagnetic interaction. Compared to $CoGeO_3$, the M1–M1 distance—of course—is larger, scaling well with the size difference between Co^{2+} and Mn^{2+}, the involved M–O–M bond angles are smaller by ∼1.0° and ∼0.5° in $MnGeO_3$. The shortest Mn^{2+}–Mn^{2+} distance within the M1/M2 band is the M1–M2 contact, which is 3.124(4) Å and approximately points in the [0 1 1] direction, a second M1–M2 distance is 3.199(4) Å, and points approximately in $[0\,1\,\bar{1}]$, these interactions are defined as J_1 and J_1' in figure 1(a), while a third M1–M2 distance exists approximately along ***b***, which amounts to 3.361(4) Å (J_2 in figure 1(a)). The shortest distances between Mn^{2+} cations between two M1 sites involve the tetrahedral chains. As there are two distinct GeO_4 chains, one has to discern between two different shortest distances between M1/M2 bands: along the GeA sites the shortest Mn1–Mn1 distance is 6.280(3) Å, along the GeB sites it is 5.755(4) Å.

The monoclinic modification of $MnGeO_3$ crystallizes in space group *C*2/*c*. The structure is characterized by only one distinct chain of corner-sharing GeO_4 tetrahedra. This implies that there are only three distinct oxygen atom positions in the asymmetric unit and thus only three instead of six different Mn1–O and Mn2–O distances in monoclinic $MnGeO_3$. From the strong kinking of the tetrahedral chains with an O3–O3–O3 angle of 129.3(1)°, the $MnGeO_3$ structure can be classified as *HP*-*C*2/*c*, i.e. it is isotypic to the high pressure *C*2/*c* structure of the silicate pyroxenes. The M1 octahedra, forming zigzag chains parallel to the ***c***-axis similar to the ones in the orthorhombic modification, are quite regular with ⟨Mn1–O⟩ = 2.21(2) Å (the large estimated standard deviation in monoclinic $MnGeO_3$ are due to the low phase content in the total sample). The shortest Mn1–Mn1 distance is 3.24(1) Å, the M1–O1–M1 bond angle = 91.3(2)°, so evidently closer to a 90° geometry than in the orthopyroxene. The M2 sites with ⟨Mn2–O⟩ = 2.21(2) Å are again attached laterally to each side of the M1 chain, so that a central M1 site has three next nearest neighbouring M2 sites with M1–M2 distances ranging between 3.09(2) and 3.49(2) Å. The shortest distance between M1 sites in two different chains via the tetrahedral sites is 5.82(2) Å, which is similar to the value found along the GeB pathway in orthorhombic form of $MnGeO_3$. More detailed descriptions of the general structural topology in equally sized M1/M2 cation germanate pyroxenes can be found in [9].

3.2. Temperature evolution of the nuclear structure

There is no crystallographic phase transition down to the lowest measured temperature, i.e. both modifications retain their *Pbca* and *C*2/*c* symmetry down to 4 K. For the orthorhombic modification, lattice parameters ***a***, ***b*** and ***c*** decrease with temperature following a simple Einstein relation with low temperature saturation beginning below 200 K. Constant thermal expansion is reached above 550(7) K, 400(11) K and 422(8) K along ***a***, ***b*** and ***c***, respectively. Above these temperatures, linear thermal expansion coefficients can be calculated as $\alpha_a = 7.3(3) \times 10^{-5}$ K^{-1}, $\alpha_b = 11.3(4) \times 10^{-5}$ K^{-1} and $\alpha_c = 7.9(4) \times 10^{-5}$ K^{-1}. Towards lower temperature however, distinct deviations from

Table 3. Selected bond lengths (Å) and angles at some representative temperatures for synthetic $MnGeO_3$ pyroxene in the monoclinic $C2/c$ and the orthorhombic $Pbca$ form as extracted from Rietveld refinements of neutron diffraction data.

	$MnGeO_3$ $Pbca$			$MnGeO_3$ $C2/c$		
Temp (K)	4	50	298	4	50	298
Mn1–O1A (Å)	2.152(4)	2.157(3)	2.155(3)	2.36(3)	2.31(2)	2.36(2)
Mn1–O1B (Å)	2.170(5)	2.173(3)	2.176(3)	2.36(3)	2.31(2)	2.36(2)
Mn1–O1A (Å)	2.230(5)	2.227(4)	2.238(4)	2.16(1)	2.156(8)	2.161(9)
Mn1–O1B (Å)	2.262(5)	2.259(4)	2.269(4)	2.16(1)	2.156(8)	2.161(9)
Mn1–O2A (Å)	2.116(4)	2.109(4)	2.108(4)	2.02(3)	2.16(2)	2.10(3)
Mn1–O2B (Å)	2.121(5)	2.140(4)	2.141(4)	2.02(3)	2.16(2)	2.10(3)
⟨Mn1–O⟩ (Å)	2.175	2.177	2.181	2.180	2.209	2.207
$Mn1–Mn1_{(intra)}$ (Å)	3.255(5)	3.259(4)	3.269(4)	3.32(5)	3.19(2)	3.24(2)
$Mn1–Mn1_{(GeA)}$ (Å)	6.298(5)	6.283(4)	6.280(4)	5.85(5)	5.85(2)	5.82(2)
$Mn1–Mn1_{(GeB)}$ (Å)	5.738(5)	5.752(4)	5.755(4)	5.85(5)	5.85(2)	5.82(2)
Mn1–Mn2 (Å)	3.116(5)	3.113(4)	3.125(4)	3.03(3)	3.08(2)	3.08(2)
Mn1–Mn2 (Å)	3.215(5)	3.212(4)	3.199(4)	3.03(3)	3.08(2)	3.08(2)
Mn1–Mn2 [010] (Å)	3.362(6)	3.354(4)	3.361(4)	3.56(4)	3.40(4)	3.49(4)
Mn1–O1A–Mn1	95.9(2)	96.0(1)	96.2(1)	94.3(6)	91.0(4)	91.3(4)
Mn1–O1B–Mn1	94.5(2)	94.7(1)	94.7(1)	94.3(6)	91.0(4)	91.3(4)
Mn2–O1A (Å)	2.217(6)	2.197(4)	2.192(4)	2.11(3)	2.15(2)	2.11(2)
Mn2–O1B (Å)	2.181(6)	2.171(4)	2.172(4)	2.11(3)	2.15(2)	2.11(2)
Mn2–O2A (Å)	2.162(6)	2.149(4)	2.155(4)	2.08(3)	2.10(2)	2.19(2)
Mn2–O2B (Å)	2.081(6)	2.089(4)	2.079(3)	2.08(3)	2.10(2)	2.19(2)
Mn2–O3A (Å)	2.366(5)	2.363(4)	2.282(3)	2.37(3)	2.39(2)	2.32(2)
Mn2–O3B (Å)	2.416(5)	2.433(4)	2.458(3)	2.37(3)	2.39(2)	2.32(2)
⟨Mn2–O⟩ (Å)	2.237	2.234	2.240	2.187	2.214	2.206
Ge1–O1A (Å)	1.722(4)	1.733(2)	1.737(2)	1.78(2)	1.73(1)	1.71(1)
Ge1–O2A (Å)	1.724(4)	1.716(2)	1.718(2)	1.72(3)	1.68(1)	1.70(1)
Ge1–O3A (Å)	1.754(3)	1.764(2)	1.761(2)	1.77(2)	1.77(1)	1.82(1)
Ge1–O3A (Å)	1.798(3)	1.794(2)	1.791(2)	1.85(2)	1.82(1)	1.83(1)
⟨GeA–O⟩ (Å)	1.749	1.752	1.752	1.780	1.749	1.763
O3A–O3A–O3A (deg)	160.4(1)	160.0(1)	160.3(1)	130.3(4)	131.5(4)	129.2(4)
Ge2–O1B (Å)	1.729(3)	1.746(2)	1.743(2)			
Ge2–O2B (Å)	1.723(4)	1.701(2)	1.697(2)			
Ge2–O3B (Å)	1.792(4)	1.793(2)	1.794(2)			
Ge2–O3B (Å)	1.806(3)	1.811(2)	1.815(2)			
$\langle Ge–O\rangle_B$ (Å)	1.763	1.763	1.763			
O3B–O3B–O3B (deg)	134.45(9)	134.40(8)	134.87(9)			

the low temperature saturation of lattice parameters occur. These are more gradual in character and can be assigned to magneto-elastic coupling of the structure (figures 2(a)–(c)). For orthorhombic $MnGeO_3$ the $\boldsymbol{a}$- and $\boldsymbol{b}$-axis increase with decreasing T, while along $\boldsymbol{c}$ a contraction takes place. For the monoclinic phase there are similar low temperature deviations below 40 K observed, however, they have a more discontinuous character: $\boldsymbol{a}$ increases, $\boldsymbol{b}$, $\boldsymbol{c}$ (figure 2(d)) and the monoclinic angle distinctly decrease.

For the monoclinic modification the thermal expansion tensor components were determined following the procedure described in [3, 9] giving $\alpha_a = 11.7(3) \times 10^{-5}$ K^{-1}, $\alpha_b = 8.9(4) \times 10^{-5}$ K^{-1} and $\alpha_c = 7.8(4) \times 10^{-5}$ K^{-1}. The thermal expansibility thus is different in the monoclinic modification which is, however, comparable to the observations for other $C2/c$-type germanates, e.g. $LiFeGe_2O_6$ [3].

Lowering temperature causes some small but distinct alterations in secondary structural parameters. Between room temperature and 50 K, the average ⟨Mn1–O⟩ distance in the orthorhombic phase decreases by 0.004 Å, the ⟨Mn2–O⟩ one by 0.006 Å, while the ⟨Ge–O⟩ distances remain unaltered.

Table 4. Observed fitted parameters using the Einstein model as given in equation (1) for lattice parameters of orthorhombic and monoclinic $MnGeO_3$.

	$\boldsymbol{a}$	$\boldsymbol{b}$	$\boldsymbol{c}$	$\boldsymbol{\beta}$	$\boldsymbol{V}$
$Pbca$ phase					
a_0 (Å)	19.2715(3)	9.2394(2)	5.4724(3)	—	974.21(3)
C_E	0.084(2)	0.043(1)	0.019(1)	—	11.3(2)
θ_E (K)	550(7)	400(8)	422(11)	—	425(7)
$C2/c$ phase					
a_0 (Å)	9.8994(3)	9.2588(3)	5.2684(2)	101.49(1)	473.1(2)
C_E	0.059(3)	0.025(2)	0.019(1)	0.032(4)	5.8(2)
θ_E (K)	488(13)	299(18)	441(21)	504(12)	444(12)

3.3. Magnetic spin structure of monoclinic $MnGeO_3$

Below 40 K the neutron powder diffraction patterns of $MnGeO_3$ shows an increase of the background in the 25°–45° 2θ region as well as an appearance of new Bragg peaks for temperatures <36 K. This increase in background is a typical sign for magnetic short-range ordering and frequently

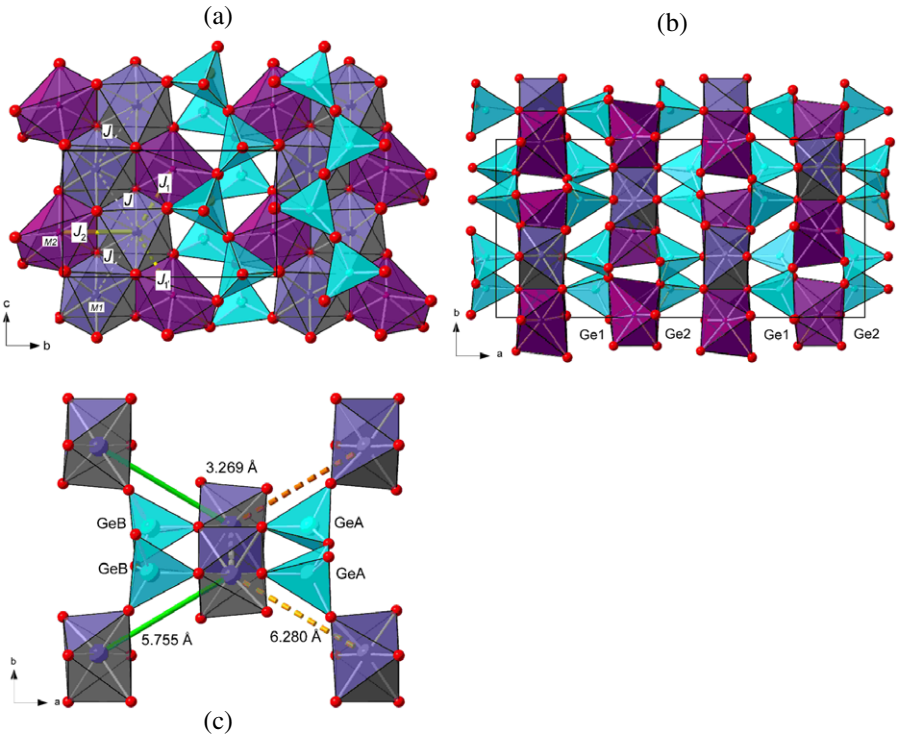

Figure 1. Polyhedral representation of the $MnGeO_3$ structure in the *Pbca* modification in two different orientations: (a) viewed along the [1 0 0] direction, the different superexchange pathways within the M1/M2 band are marked, (b) viewed along [0 0 1], (c) possible magnetic intra- and inter-chain pathways for magnetic superexchange (viewed along [0 0 1]).

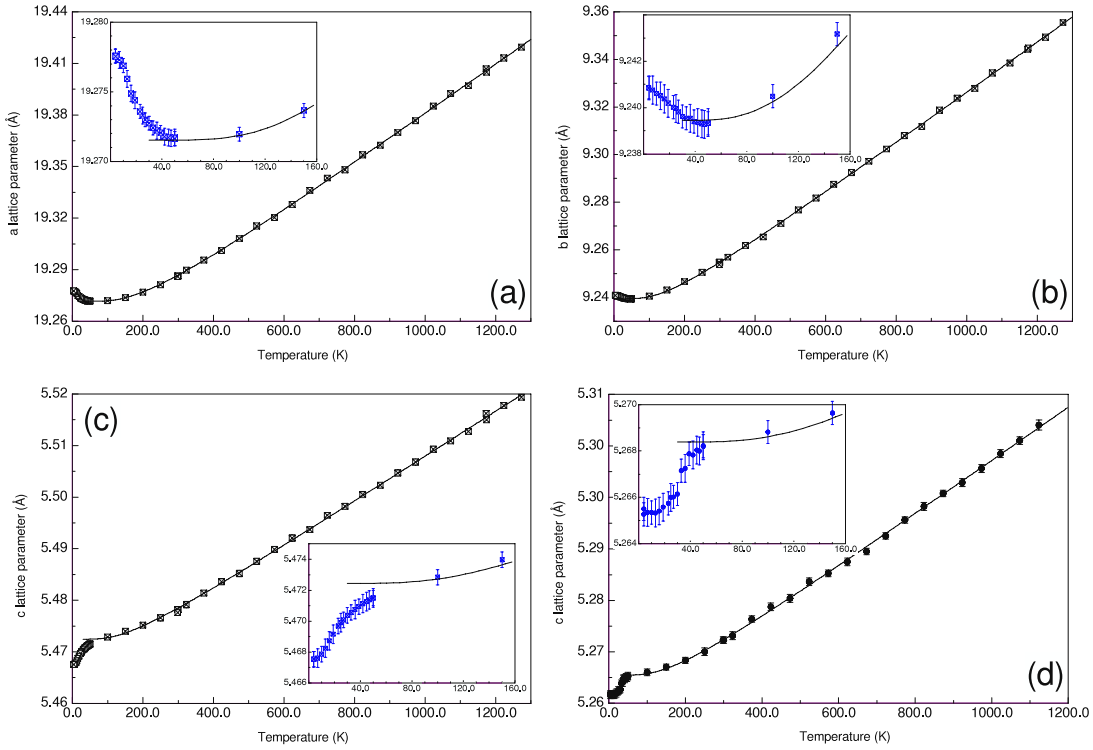

Figure 2. Evolution of lattice parameters of orthorhombic ((a)–(c)) and—as an example—of the *c*-lattice parameter of monoclinic $MnGeO_3$ (d). Data above 40 K are fitted to a simple Einstein model; the insets show the low temperature neutron diffraction data deviating from the simple behaviour due to the strong magneto-elastic coupling.

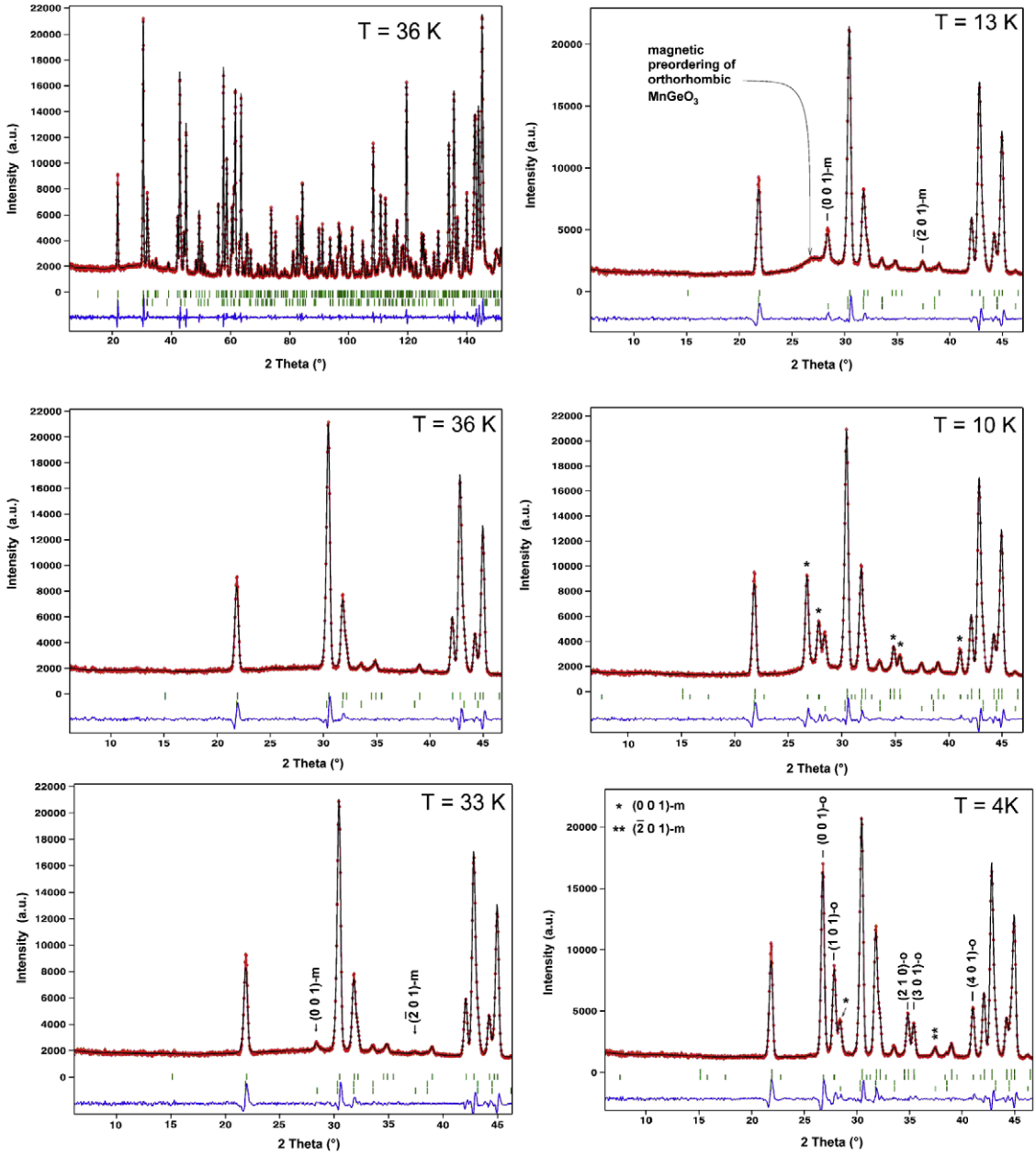

Figure 3. Full and low angle region of the neutron diffraction pattern of $MnGeO_3$, collected at different temperatures at the SPODI diffractometer with $\lambda = 2.537$ Å, prominent magnetic reflections are marked with their indices; 'm' and 'o' correspond to the monoclinic and orthorhombic phases, respectively, the stars in the $T = 10$ K pattern mark the newly appearing reflections of the magnetic ordering in the orthorhombic phase.

found in the clinopyroxenes [5, 8, 9]. The newly arising Bragg reflections could not be assigned to the orthorhombic phase of $MnGeO_3$ with any possible commensurate or incommensurate propagation vector. Contrarily, these superstructure reflections were easily ascribed to the monoclinic phase and indexed with a magnetic propagation vector $\boldsymbol{k} = (0, 0, 0)$. This means that the magnetic and the nuclear unit cell are identical. Figure 3 displays the low angle region of the powder neutron diffractograms of $MnGeO_3$. In the 13 K data (figure 3), a strong increase in the background is again occurring which is indicative of the short-range magnetic ordering of the orthorhombic (majority) phase. The latter transforms into the 3D ordered phase below about 13 K, as shown by the appearance of strong magnetic Bragg peaks (see section 3.4).

Possible magnetic structures, compatible with the $C2/c$ symmetry of monoclinic $MnGeO_3$ at low temperatures were determined by representational analysis, following the formalism of Bertaut [27] using the computer programs BasIreps [25] and SARAh [28]. The representation Γ is constructed with the Fourier components m^k corresponding to the Mn atoms at the two 4e positions $((0, y, 1/4)$ and $(0, -y, 3/4)$ with $y = 0.8981$ and $y = 0.2750$ for Mn1 and Mn2, respectively). The decomposition of Γ in terms of the

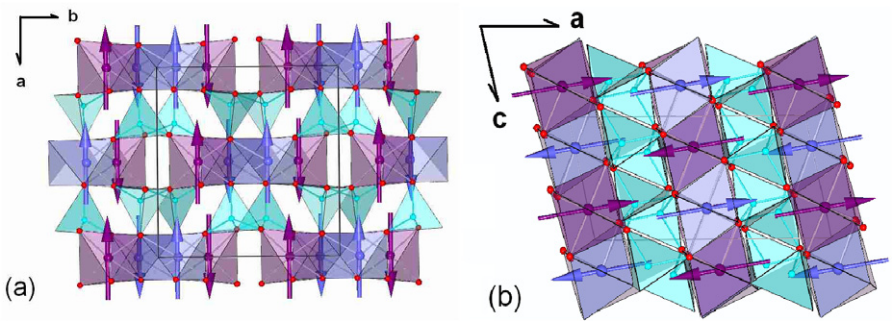

Figure 4. Magnetic structure of monoclinic MnGeO3 at 4K in two different views, blue and purple spins represent the M1 and M2 sites, respectively; (a) projected along the ***a***–***b*** plane, (b) projected onto the ***a***–***c*** plane.

Table 5. Possible magnetic structure consistent with space group $C2/c$ and $\boldsymbol{k} = (0, 0, 0)$ for transition metals on the 4e position with 4e_1 $= (0, y, 1/4)$ and 4e_2 $= (0, -y, 3/4)$ and $y = 0.8981$ and 0.2750 for monoclinic $MnGeO_3$. $F = (++)$, $A = (+-)$ of spin orientation following the notation of [27].

# IrReps	4e_1	4e_2	Basis function	Magn. S.G.
Γ1	$[0, v, 0]$	$[0, v, 0]$	$(0, F_y, 0)$	$C2/c$
Γ2	$[0, v, 0]$	$[0, -v, 0]$	$(0, A_y, 0)$	$C2/c'$
Γ3	$[u, 0, w]$	$[u, 0, w]$	$(F_x, 0, F_z)$	$C2'/c'$
Γ4	$[\mathbf{u}, \mathbf{0}, \mathbf{w}]$	$[-\mathbf{u}, \mathbf{0}, -\mathbf{w}]$	$(\mathbf{A}_x, \mathbf{0}, \mathbf{A}_z)$	$C2'/c$

irreducible representation Γ_k for the 4e site is given as

$$\Gamma(4e) = 1\Gamma_1 + 1\Gamma_2 + 2\Gamma_3 + 2\Gamma_4. \quad (2)$$

The different basis vectors, which are associated with each irreducible representation were also calculated with the program BasIreps [25] using the projection operator technique. Table 5 gives the possible magnetic structures, consistent with the $C2/c$ symmetry and the resulting magnetic space groups, as determined from [29]. We assumed that the moments on M1 and M2 are strongly coupled and thus the modes at M1 and M2 belong to the same representation.

According to the refinements of the 16 K data the magnetic structure of monoclinic $MnGeO_3$ is given by the irreducible representation Γ4 with the basis functions $(A_x, 0, A_z)$, while all other models clearly fail to fit the experimental data. The obtained magnetic space group is $C2'/c$. The refinements yield a model of the magnetic structure with the spins aligned within the ***a***–***c*** plane for both sites; thereby the components of the magnetic moments m_x and m_z were very similar in totally unconstrained refinements, yielding similar total magnetic moments (with M2 being slightly higher, but still within two times the estimated standard deviation) and almost identical spin orientations of 92(1)° and 89(1)° at 4 K for M1 and M2 within the ***a***–***c*** plane. Due to the low amount of monoclinic phase it thus was decided to constrain the magnetic moment on M1 and M2 to have the same value and orientation in order to reduce refinement parameters of the magnetic model. Drawings of the obtained magnetic structure are displayed in figure 4. Within the chains of M1 octahedra, the spins are collinear and have an antiferromagnetic alignment. The magnetic moment vector forms an angle of 92(1)° with the ***c*** axis, without a clear temperature dependence. However there are no clear indications for a distinct spin rotation with temperature. The coupling of spins between the M1 chains is also antiferromagnetic. The magnetic moments on the M2 sites are anti-parallel to the ones at M1 (figure 4) via the J_1 and J_1' interaction, but have the same orientation, also in unconstrained refinements. This is different to isotypic $CoGeO_3$, where spins are rotated away from each other by ∼50° [9]. The antiferromagnetic interaction between M1 and M2 sites along J_1 and J_1' results in a parallel spin-alignment between neighbouring M1 and M2 sites along the ***b***-axis (compare figures 4(a) and 5(b)), i.e. along the J_2 interaction, which involves the long M1–M2 distance and certainly causes magnetic frustration.

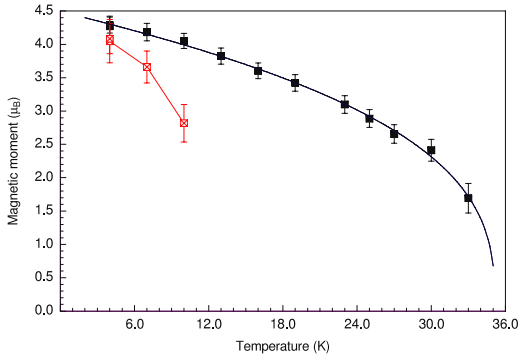

Figure 5. Variation of the total magnetic moment in $MnGeO_3$ as a function of temperature: filled squares, monoclinic $MnGeO_3$; open crossed squares, orthorhombic $MnGeO_3$.

The total magnetic moment on M1 and M2 yields a value of 4.29(9) μ_B at 4 K. This is a distinct reduction of ∼27% to the theoretical spin-only value of 5.92 μ_B of Mn^{2+} [30], which may be due to magnetic frustration. The data for the total magnetic moment for monoclinic $MnGeO_3$, derived from the neutron diffraction data, are displayed in figure 5. They were fitted with a phenomenological power law $M(T) = M(0)^*[1-(T/T_N)^\alpha]^\beta$ [31] which forces a $M(T) \propto [1 - (T/T_N)]^\beta$ behaviour in the critical region near T_N while a $M(T) = M(0)^*[1 - cT^\alpha]$ behaviour is obtained at $T \to 0$ [31]. For the monoclinic phase these fittings yield $M(0) = 4.49(1)$ μ_B, $T_N = 35.1(1)$ K, $\alpha = 1.0(2)$ and a critical exponent $\beta =$

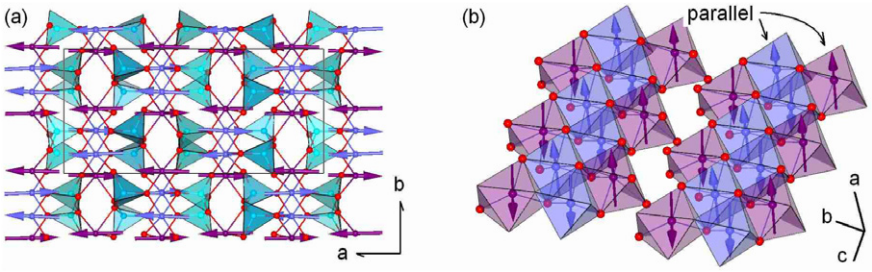

Figure 6. Magnetic structure of orthorhombic $MnGeO_3$ at 4K, blue and purple spins represent the M1 and M2 sites, respectively: (a) projection along $\boldsymbol{c}$, (b) three-dimensional view.

0.34(3); the critical exponents β is consistent with a 3D model of ordering.

Monoclinic $MnGeO_3$ has the same structural topology as $CaMnGe_2O_6$, except that the M2 site is occupied by the larger Ca^{2+} (1.12 Å) as compared to Mn^{2+} (0.82 Å) thus increasing the chain separation to 5.903(6) Å [5], while the Mn^{2+}–Mn^{2+} distance within the M1 chain is similar to monoclinic $MnGeO_3$. The Ca compound however has a distinctly lower magnetic ordering temperature of 11.6(2) K. The magnetic spin structure is remarkably similar. It can be described in space group $C2'/c$ with $k = (0, 0, 0)$, yielding a pure antiferromagnetic spin arrangement. The magnetic moments are aligned within the $\boldsymbol{a}$–$\boldsymbol{c}$ plane forming an angle of 88.4° with the crystallographic $\boldsymbol{c}$-axis. This is almost the same angle as found in monoclinic $MnGeO_3$, thus the increase of M1-chain separation does hardly influence the magnetic spin structure but only reduces the magnetic ordering temperature by ∼22 K being in line with $CaCoGe_2O_6$ [5] and monoclinic $CoGeO_3$ [9]. Here the replacement of Co^{2+} on M2 by Ca^{2+} reduced the ordering temperature by ∼17.5 K, keeping also the magnetic spins structure almost unaltered, except some more pronounced spin rotations within the $\boldsymbol{a}$–$\boldsymbol{c}$ plane. The total magnetic moment in $CaMnGe_2O_6$ is 4.10(4) μ_B at 1.4 K and of similar size as in the title compound.

3.4. Magnetic spin structure of orthorhombic $MnGeO_3$

For the (two-phased) $MnGeO_3$, no new Bragg reflections appear in the neutron diffraction pattern between 33 and 13 K, despite the facts that the magnetic reflections of monoclinic $MnGeO_3$ gain intensity and a distinct increase of the background in the 25°–40° 2θ region occur, indicative of magnetic pre-ordering phenomena in the orthorhombic phase. Intense additional magnetic Bragg peaks appear at 10 K (figure 3). They can be indexed on the basis of the nuclear unit cell of the orthorhombic phase with magnetic propagation vector $\boldsymbol{k} = (0, 0, 0)$. Possible magnetic structures compatible with the $Pbca$ symmetry of orthorhombic $MnGeO_3$ were again calculated using representational analysis. The representation Γ now is constructed with the Fourier components m_k corresponding to Mn^{2+} on the two general positions 8c. The decomposition of Γ in terms of the irreducible representation Γ_k for the 8c site is given as

$$\Gamma(8c) = 1\Gamma_1 + 1\Gamma_2 + 2\Gamma_3 + 2\Gamma_4. \quad (3)$$

Table 6. Possible magnetic structures, consistent with space group $Pbca$ and $\boldsymbol{k} = (0, 0, 0)$ for Mn on the 8c position in orthorhombic $MnGeO_3$ and corresponding magnetic space groups according to [29]. $F^+ = (++++, ++++)$, $F^- = (++++, ----)$, $G = (+-+-)$, $A(+--+)$, $C = (++--)$ following the notation of [27].

# IrReps	x	y	z	Magn. S.G.
Γ1	A_x^-	G_y^-	C_z^-	$Pb'c'a'$
Γ2	A_x^+	G_y^+	C_z^+	$Pbca$
Γ3	G_x^-	A_y^-	F_z^-	$Pbca'$
Γ4	$\mathbf{G}_x^+$	$\mathbf{A}_y^+$	$\mathbf{F}_z^+$	$\boldsymbol{Pb'c'a}$
Γ5	C_x^-	F_y^-	A_z^-	$Pbc'a$
Γ6	C_x^+	F_y^+	A_z^+	$Pb'ca'$
Γ7	F_x^-	C_y^-	G_z^-	$Pb'ca$
Γ8	F_x^+	C_y^+	G_z^+	$Pbc'a'$

Table 6 gives the eight different possible magnetic structures, compatible with the $Pbca$ space group. Again it is assumed that M1 and M2 sites order simultaneously and thus belong to the same representation. However, we have also tested different combinations of Γ on M1 and M2 during the Rietveld refinements. Best results however were obtained for a model given by the representation Γ4 on both sites having the basis functions $[G_x^+, A_y^+, F_z^+]$ with magnetic space group $Pb'c'a$, allowing the magnetic moment vector to have components along all three crystallographic axes. Diagrams of the magnetic structure are displayed in figure 6.

Refinement on the 4 K data yields a pure antiferromagnetic ordering in $MnGeO_3$, the components of the magnetic moment vector along $(\boldsymbol{m}_x, \boldsymbol{m}_y, \boldsymbol{m}_x)$ are compiled in table 7. In unconstrained refinements, these components were identical within experimental error on M1 and M2 at any temperature, thus it was decided to fix them to have the same values on M1 and M2 in subsequent refinements. This is justified in terms of unaltered resulting agreement factors and helps to keep the magnetic model as simple as possible. Following from the refined values of $\boldsymbol{m}$, the magnetic spins are aligned almost perfectly along the crystallographic $\boldsymbol{a}$-axis with only very small rotations of ∼1.5(9)° towards the $\boldsymbol{c}$-axis, the coupling is antiferromagnetic within and between the M1 chains and the total magnetic moments amounts 4.05(6) μ_B. The spins on M2 also have anti-parallel alignment to the neighbouring M1 sites via the shorter J_1 and J_1' interaction; as for the monoclinic case, however, there is a parallel moment orientation between Mn^{2+} ions on M1 and M2 along the $\boldsymbol{b}$-axis (via the J_2 path). The

Table 7. Ordering temperatures, components and resulting total magnetic moments in synthetic $MnGeO_3$ polymorphs as extracted from Rietveld refinements on neutron diffraction data (values on M1 and M2 were constrained to be equal during refinement).

	$CaMnGe_2O_6$ [a]	$MnGeO_3$ cpx	$MnGeO_3$ opx
T_N (K)	11.6(2)	35.1(2)	∼12
Mx (M1) (μ_B)	4.23(2)	4.37(11)	4.05(7)
My (M1) (μ_B)	—	—	0.00(5)
Mz (M1) (μ_B)	1.14(2)	0.62(11)	0.10(5)
M_{M1} (μ_B)	4.10	4.29	4.06
$\angle(c, M_{M1})$ (deg)	88.4(5)	92.0(8)	91.5(5)
J in chain	AFM	AFM	AFM
J between chains	AFM	AFM	AFM
Magn. space group	$C2'/c$	$C2'/c$	$Pb'c'a$

[a] Data recalculated from [5], T_N = Néel temperature, $\angle(c, M_{M1})$ = angle between the magnetic moment at the M1 site and the crystallographic c-axis.

total magnetic moment on M1 and M2 is reduced by ∼31% to the theoretical spin-only value of Mn^{2+} indicative for distinct magnetic frustration, probably due to the ferromagnetic spin orientation along $\boldsymbol{b}$. The variation of the total magnetic moment is included in figure 5; however it was not possible to perform a fit due to the small number of low temperature data-points available. Evidently, saturation of magnetic moments is not yet reached at 4 K in the $Pbca$ modification, but also the $C2/c$ form still shows an increase in the magnetic moment at low temperatures. Our model of the magnetic structure in orthorhombic $MnGeO_3$ is in perfect agreement with the one of Herpin *et al* [21], who also proposed the spins oriented along the long crystallographic axis ($\boldsymbol{b}$ in their setting), their magnetic moments at 4 K are 4.27 and 4.04 μ_B for M1 and M2, respectively, also in good accordance with the data of this study.

4. Conclusions

Similar to $CoGeO_3$, the pyroxene-type compound $MnGeO_3$ exists in two different modifications, a monoclinic one with $C2/c$ symmetry and an orthorhombic one with space group $Pbca$. The sample, studied by neutron diffraction, contained ∼9 wt% of the monoclinic phase as an impurity, yet we were able to solve the magnetic structures of both compounds. During an *in situ* high temperature x-ray diffraction data collection, we observed a disappearance of the monoclinic phase at ∼1123 K, indicative of a non-reversible monoclinic to orthorhombic phase transition, however, we found no transition around 473 K, where the orthorhombic to monoclinic phase transition was proposed to occur.

The nuclear structures of both $MnGeO_3$ modifications are similar to the pyroxene-type compounds $CoGeO_3$ [9]. The main differences between the two $MnGeO_3$ forms concern the M1–M1 chain separations, which are distinctly larger along the GeA pathway (6.280 Å) in the orthorhombic modification, as compared to the monoclinic form with a shortest M1–M1 distance between the chains of 5.820 Å, thus lowering the magnetic ordering temperature by ∼22 K. While the $C2/c$ form orders magnetically around 34 K, the $Pbca$ modification transforms to the ordered state below 13 K.

As our sample was prepared in air in a platinum crucible, we can rule out the presence of Si^{4+} at the tetrahedral sites; nevertheless we find a low ordering temperature of the $Pbca$ modification of $MnGeO_3$, which is in good agreement with the results of Herpin *et al* [21], but disagrees with the ordering temperatures of ∼38 K given in [19]. One explanation might be that the sample of [19] is the monoclinic modification with $T_N \sim 34$ K; however this contrasts the single crystal structure refinement of [19], where the authors state that they have determined the orthorhombic modification[5]. So at the moment we have no explanation for the discrepancy in magnetic ordering temperatures, but can only fix the ordering temperatures of the $C2/c$ and $Pbca$ modifications in our sample with ∼34 K and ∼12 K, respectively.

The magnetic structures of the two modifications are similar to each other. The orthorhombic modification possesses a simple antiferromagnetic spin structure with the magnetic moments aligned along the $\boldsymbol{a}$-axis. The M1 sub-lattice has pure anti-parallel spin-alignment within and between the M1 chains, though the M–O–M angles are closer to the 90°, favouring ferromagnetic interaction [32], than in $CoGeO_3$, the latter having ferromagnetically ordered spins within the M1 chains [9]. However there is a small ferromagnetic interaction of Mn^{2+} on M1 and M2 for the superexchange along the $\boldsymbol{b}$-axis which may cause magnetic frustration and the distinct reduction of the total magnetic moment.

There is a remarkable small influence of the substitution of Mn^{2+} by the diamagnetic Ca^{2+} on M2 onto the spin structure of Mn^{2+} on the M1 sites. The magnetic spins structures in monoclinic $MnGeO_3$ and $CaMnGe_2O_6$ are almost identical with only the ordering temperature being higher in $MnGeO_3$ by ∼22 K.

Acknowledgments

Neutron diffraction experiments have been supported by the European Commission under the 7th Framework programme through the 'Research Infrastructures' action of the 'Capacities' programme, Contract No. CP_CSA_Infra-2008-1.1.1 Number 226507-NIMI3.

References

[1] Cameron M and Papike J J 1981 *Am. Mineral.* **66** 1–50
[2] Redhammer G J and Roth G 2004 *Z. Kristallogr.* **219** 585–605
[3] Redhammer G J, Cámara F, Alvaro M, Nestola F, Tippelt G, Prinz S, Simons J, Roth G and Amthauer G 2010 *Phys. Chem. Mineral.* **37** 685–704
[4] Jodlauk S, Becker P, Mydosh J A, Khomskii D I, Lorenz T, Streltsov S V, Hezel D C and Bohaty L 2007 *J. Phys.: Condens. Matter* **19** 432201
[5] Redhammer G J, Roth G, Treutmann W, Paulus W, André G, Pietzonka C and Amthauer G 2008 *J. Solid State Chem.* **181** 3163–76

[5] In [19], the authors note that the orthorhombic form is stable up to 900 °C, without giving further information on the nature of a possible transition. This temperature however is similar to the temperature where the monoclinic $MnGeO_3$ to orthorhombic $MnGeO_3$ transition was found in this present study.

[6] Nenert G, Ritter G, Isobe M, Isnard O, Vasiliev A N and Ueda Y 2009 *Phys. Rev.* B **80** 024402
[7] Redhammer G J, Roth G, Paulus W, André G, Lottermoser W, Amthauer G, Treutmann W and Koppelhuber-Bitschnau B 2001 *Phys. Chem. Mineral.* **28** 337–46
[8] Redhammer G J, Roth G, Treutmann W, Hoelzel M, Paulus W, André G, Pietzonka C and Amthauer G 2009 *J. Solid State Chem.* **182** 2374–84
[9] Redhammer G J, Senyshyn A, Tippelt G, Pietzonka C, Roth G and Amthauer G 2010 *Phys. Chem. Mineral.* **37** 311–31
[10] Redhammer G J, Ohashi H and Roth G 2003 *Acta Crystallogr.* B **59** 730–46
[11] Isobe M, Nimomiya E, Vasil'ev A N and Ueda Y 2002 *J. Phys. Soc. Japan* **71** 1423–6
[12] Redhammer G J, Pachler A, Hoelzel M, Tippelt G, Roth G and Amthauer G 2011 *Phys. Chem. Mineral.* **38** 139–57
[13] Nenert G, Isobe M, Ritter C, Isnard O, Vasiliev A N and Ueda Y 2009 *Phys. Rev.* B **79** 064416
[14] Nenert G, Kim I, Isobe M, Ritter C, Vasiliev A N, Kim K H and Ueda Y 2010 *Phys. Rev.* B **81** 184408
[15] Grodzicki M, Redhammer G J, Reissner M, Steiner W and Amthauer G 2010 *Phys. Chem. Mineral.* **37** 11–23
[16] Streltsov S V, McLeof J, Moewes A, Redhammer G J and Kurmaev E Z 2010 *Phys. Rev.* B **81** 045118
[17] Tauber A, Kohn J A, Whinfrey C G and Babbage W D 1963 *Am. Mineral.* **48** 555–64
[18] Fang J A and Townes W D 1969 *Z. Kristallogr.* **130** 139–47
[19] Sapronova N V, Volkov N V, Sablina K A, Petrakovskii G A, Bayukov O A, Vorotynov A M, Velikanov D A, Bovina A F, Vasilyev A D and Bondarenko G V 2009 *Phys. Status Solidi* b **246** 206–14
[20] Matsumura H, Mamiya M and Takei H 2000 *J. Cryst. Growth* **210** 783–7
[21] Herpin P, Whuler A, Boncher B and Sougi M 1971 *Phys. Status Solidi* b **44** 71–84
[22] Brown J P, Forsyth B J and Tasset F 2005 *Solid State Sci.* **7** 682–9
[23] Becker U W and Felsche J 1987 *J. Less-Common Met.* **128** 269–80
[24] Hoelzel M, Senyhyn A, Gilles R, Boysen H and Fuess H 2007 *Neutron News* **18** 23–6
[25] Rodríguez-Carvajal J 2001 Recent developments of the program FULLPROF *Newsletter of the Commission on Powder Diffraction* **26** 12–9
[26] Yamanaka T, Hirano M and Takéuchi Y 1985 *Am. Mineral.* **70** 365–74
[27] Bertaut E F 1968 *Acta Crystallogr.* A **24** 217–31
[28] Wills A S 2000 *Physica* B **276–278** 680–1
[29] Litvin D B 2008 *Acta Crystallogr.* A **64** 419–24
[30] Lueken H 1999 *Magnetochemie. Eine Einführung in Theorie und Praxis* (*Teubner Studienbücher, Chemie*) (Stuttgart: Teubner) p 509
[31] Blundell S J, Steer C A, Pratt F L, Marshall I M, Hayes W and Ward R C C 2003 *Phys. Rev.* B **67** 224411
[32] Goodenough J B 1963 *Magnetism and the Chemical Bond* (New York: Wiley)